Rombohedral heterometallic alkynyl based Pt_2Cd_2 clusters: Structural, photophysical and theoretical studies.

Jesús R. Berenguer, Julio Fernández, Belén Gil, Elena Lalinde* and Sergio Sánchez.

Departamento de Química-Grupo de Síntesis Química de La Rioja, UA-CSIC, Universidad de La Rioja, 26006, Logroño, Spain.

Abstract

Reactions between $[Pt(C{\equiv}CR)_4]^{2-}$ (R = Tol **a**, C_6H_4OMe-4 **b**, C_6H_4OMe-3 **c**) and Cd^{2+} depend on the media and the alkynyl substituent, leading to the formation of yellow tetranuclear solvate complexes $[Pt(C{\equiv}CR)_4Cd(acetone)]_2$ **1a**,**b(acetone)$_2$** and $[Pt(C{\equiv}C C_6H_4OMe\text{-}3)_4Cd(dmso)]_2$ **1c(dmso)$_2$** or white polymeric solvate free species $[Pt(C{\equiv}CR)_4Cd]_x$ **1'a-c**. Treatment of **1a**,**b(acetone)$_2$** or **1'a-c** with N-donor ligands affords a series of tetranuclear clusters $[Pt(C{\equiv}CR)_4CdL]_2$ (L = py; **2a-c**. R = Tol; L = $NC_5H_4CH_3$-4 **3**, $NC_5H_4CF_3$-4 **4**, pzH **5**). X-ray crystallographic studies reveal that, in the tolyl complexes (**2a**, **4** and **5**), the Cd-L^{2+} unit is closely bonded to one Pt-C_α(acetylide) bond (Pt-Cd = 2.7, Cd-C_α ~ 2.48 Å), and the resulting "$Pt(C{\equiv}CTol)_4CdL$" unit dimerizes by two additional η^2-Cd-acetylide and a weaker Pt···Cd bonding interaction leading to a planar asymmetrical rombohedral metal core. By contrast, the *m*-methoxyphenyl derivatives (**2c**, **1c(dmso)$_2$**) form symmetrical Pt_2Cd_2 cores, with each Cd bonded to the incoming ligand (pyridine **2c**, dmso **1c(dmso)$_2$**) and four Pt-C_α bonds (Pt-Cd ~ 2.85; Cd-C_α 2.470(10)-2.551(5) Å) of different Pt^{II} fragments. Evidence from ligand dissociation was found for the solvate (**1a,b(acetone)$_2$**, **1c(dmso)$_2$**) and $NC_5H_4CF_3$-4 (**4**) derivatives by NMR and UV-Vis absorption spectra. All tetranuclear aggregates exhibit bright blue to green luminescence in solid state.TD-DFT calculations

were performed to shed light on the nature of the electronic transitions. In the solvate **1a**,**b(acetone)**$_2$ and **1c(dmso)**$_2$, emissions have been assigned to a platinum-alkynyl to cadmium charge transfer (^{3}MLM'CT), mixed with some intraligand ^{3}IL(C≡CR) character In the imine derivatives **2-5**, it is suggested to come from an excited state of large Pt(d)/πC≡CR→π*(imine) MLL'CT character, mixed with some Pt(d)/π(C≡CR)→Pt$_2$Cd$_2$/π*C≡CR (ML'M'CT) contribution.

Introduction

Transition metal alkynyl complexes are a continued focus of present research owing to their structural diversity, chemical reactivity and their numerous implications in the field of fundamental and applied materials science.[1] In particular, alkynyl ligands have been widely used in the design of luminescent materials with interesting and useful spectroscopic properties.[2-11] In these systems, emissive manifolds can be successfully controlled by changing the metal and coligands, and the emission energies can be additionally modulated by variation of the fragment and substituents on the carbon sp chain.

On the other hand, homo and heteropolynuclear aggregates containing closed or pseudo closed shell (d^{10}, d^8, $d^{10}s^2$) metal ions belong to a new class of luminescent materials.[12] In some of these systems, the presence of metallophilic bonds is essential to produce luminescence which, in its turn, is very sensitive to the arrangement of the metals and coligands, both in the ground and excited states. In fact, considerable experimental work has shown that metallophillic interactions play a significant role in the structure and luminescent properties of alkynyl complexes of Cu^I, Ag^I, Au^I, Hg^{II} (d^{10})[2,4-7] and Pt^{II}(d^8)[7,13,14] metal complexes. Heteropolynuclear complexes containing alkynyl bridging ligands have received much less attention and, in particular, their optical

properties have been investigated to a significant less extent.[5,9,15-17] Within this field, we and others have demonstrated that homoleptic $[Pt(C{\equiv}CR)_4]^{2-}$ [18-28] and mixed $[Pt(R_f)_2(C{\equiv}CR)_2]^{2-}$ [29-33] or $[Pt(bzq)(C{\equiv}CR)_2]^{-}$ [23,34-36] alkynyl platinates are excellent building blocks for the synthesis of heteropolynuclear Pt-M (M = d^{10}, s^2) complexes, which showed, not only interesting structures, but also very rich spectroscopic and photo-luminescent properties. In these systems, the presence of π electronic density on the alkynyl ligands and the electron-rich platinum(II) center (d^8) have allowed us to observe that, depending on the Lewis-acidic metal and the platinate substrate, the final heterometallic aggregates are mainly stabilized: a) by η^2-alkynyl-M bonds and Pt⋯M secondary interactions or b) by significant Pt-M bonds and/or secondary η(alkyne)⋯M bonds.

Thus, with d^{10} Lewis-acidic centers, while coinage metal such as Cu^I or Ag^I exhibit a remarkable preference for the electron-rich alkynyl entities,[18,20,24,33,36-38] the divalent Cd^{II} shows a delicate compromise between its affinity to form $Pt^{II}{\rightarrow}Cd^{II}$ bonds with a significant donor-acceptor character and its stabilization by unusual η(alkyne)⋯Cd^{II} bonding interactions.[19,21,29,30,39] For example, $Cd(NO_3)_2$ reacts with the *cis*- configured complexes $[cis\text{-}Pt(R_f)_2(C{\equiv}CR)_2]^{2-}$ to form unusual trimetallic $\{Pt_2Cd\}^{2-}$ species featuring only twezer-like η^2(alkyne)-Cd bonds.[29] However, in the presence of polyimine auxiliary ligands the generated "$Cd(N\text{-}N)_2^{2+}$" and "$Cd(trpy)^{2+}$" units shift towards the platinum center, contacting with both C^{α} atoms and the basic Pt^{II} (Pt⋯Cd 3.00-3.11 Å)[30] centers and, curiously, the "$Cd(cyclen)^{2+}$" unit forms a bimetallic complex $[cis\text{-}Pt(R_f)_2(C{\equiv}CPh)_2Cd(cyclen)]$ featuring a very short Pt→Cd bond (2.764(1) Å) and retaining only a weak interaction with one of the alkynyl fragments.[39] This difference between coinage M^+ ions and Cd^{2+} is probably due to the softer Lewis acidity

of the former, allowing them for stronger and/or better interaction with the π electron density of the alkynyl units.

Within this area, some time ago[21] we found that the neutralization reaction of $[Pt(C{\equiv}CPh)_4]^{2-}$ with $Cd(ClO_4)_2{\cdot}6H_2O$ yields an insoluble material of the expected stoichiometry $[PtCd(C{\equiv}CPh)_4]_n$ **A** as a white solid. Based on the relative large shift of the ν(C≡C) stretching vibration relative to the precursor ($\Delta\nu \approx 30$ cm^{-1}), it was suggested to have a polymeric nature, probably based on alkynyl platinate units acting as *bis*(chelating) bridging ligands between naked cadmium centers. Attempts to obtain crystals only caused partial hydrolysis, yielding a very unusual decanuclear cluster $[Pt_4Cd_6(C{\equiv}CPh)_4(\mu\text{-}C{\equiv}CPh)_{12}(\mu_3\text{-}OH)_4]$ (yellow crystals) stabilized not only by bridging hydroxi groups, but also by Pt···Cd and η^2-Cd-acetylide interactions.[21] As an extension of this work, we thought it would be of interest to study the neutralization reactions of other homoleptic derivatives $[Pt(C{\equiv}CAr)_4]^{2-}$, containing electron donating groups (Ar = Tol, C_6H_4OMe-4, C_6H_4OMe-3), with $Cd(ClO_4)_2{\cdot}6H_2O$ and to investigate the reactivity of the resulting neutral Pt-Cd systems towards some nitrogen donor ligands with a two-fold objective: (1) to prepare some new hetero-metallic homoleptic $\{Pt(C{\equiv}CR)_4Cd\}_n$ aggregates, which allow us to a better characterization of this kind of systems, and (2) to get access to novel neutral alkynyl based $\{Pt(C{\equiv}CR)_4CdL_x\}_n$ compounds to know whether simple N-donor ligands would have some influence and be able to tune the luminescence properties.

In this contribution, we report the preparation and optical properties of a series of some solvate $[Pt(C{\equiv}CR)_4Cd(acetone)]_2$ **1(acetone)$_2$** (R = Tol **1a**; C_6H_4OMe-4 **1b**) and unsolvated complexes $[Pt(C{\equiv}CR)_4Cd]_x$ **1'** (R = Tol **1'a**; C_6H_4OMe-4 **1'b**; C_6H_4OMe-3 **1'c**), and a series of tetranuclear clusters $[Pt(C{\equiv}CR)_4CdL]_2$ (L = py, R = Tol **2a**; C_6H_4OMe-4 **2b**; C_6H_4OMe-3 **2c**. R = Tol, L = $NC_5H_4CH_3$-4 **3**; $NC_5H_4CF_3$-4 **4**; $N_2C_3H_4$

(pzH) **5**). In addition, Time Dependent Density Functional Theory (TD-DFT) calculations were carried out on **1c(dmso)**$_2$, **2a**, **2c**, **4** and **5**, with the aim to characterize the highest few occupied and lowest few unoccupied molecular orbitals, thus getting some insight into the nature of their photophysical properties.

Experimental Section

Materials and methods: Complete details concerning the synthesis, spectroscopic characterization of **1**–**5** and computational TD-DFT calculations are provided as Supporting Information. All reactions were carried out under argon atmosphere using solvents from a solvent purification system (MBRAVW MB SPS-800).

X-ray Crystallography: Details of the structural analyses for all complexes are summarized on Table 1. Yellow crystals of **1c(dmso)**$_2$ were obtained by slow diffusion of Et_2O into a saturated solution of **1'c** in dmso/CH_2Cl_2 1:1. For **2a**, **2c** and **5**, yellow crystals were grown by slow evaporation at 0ºC of the corresponding solutions of the complexes in CH_2Cl_2 (**2a**, **2c**) or CH_2Cl_2/acetone 1:1 (**5**). Finally, greenish yellow crystals of **4** were obtained by cooling at -30ºC a mixture of **4** and $NC_5H_4CF_3$-4 in CH_2Cl_2. One (**1c(dmso)**$_2$, **2a**) or 0.5 (**2c**, **4**) molecules of CH_2Cl_2 and one molecule of acetone (**5**) were found in the corresponding asymmetric units. Also, for **5**, the existence of weak hydrogen interactions between the N-H of the pyrazol ligand and the oxygen atom of the acetone was confirmed. X-ray intensity data were collected with a NONIUS-κCCD area-detector diffractometer, using graphite-monochromatic Mo-K_α radiation. Images were processed using the DENZO and SCALEPACK suite of programs,[41] and the structures were solved by Direct Methods using SHELXS-97.[42] The absorption correction was performed using MULTI-SCAN[43] (**2a**, **2c**, **4** and **1c(dmso)**$_2$) or XABS2[44] (**5**), using the program suite WINGX.[45] The structures were refined by full-matrix least squares on F^2 with SHELXL-97,[42] and all non-hydrogen atoms were

assigned anisotropic displacement parameters. For complex **5**, and in order to establish the position for the N(N-H) atom of the pzH ligand, the structure was refined in three different ways (with the identities of the C and N in one position, reversed, and with 50/50 hybrid scattering factor at each of the affected atomic sites). Examination of the ΔMSDA values for bonds involving these atoms,[46,47] revealed the correct assignment, which is shown in the Figure 2. The hydrogen atoms were constrained to idealized geometries fixing isotropic displacement parameters 1.2 times the U_{iso} value of their attached carbon for the aromatic and 1.5 times for the methyl groups. Several restrains have been used to model the CH_2Cl_2 molecule in **1c(dmso)$_2$** and the positional disorder present by the CF_3 group of the $NC_5H_4CF_3$-4 ligand in **4**. Finally, all the structures present some residual peaks greater than 1 eA^{-3} in the vicinity of the platinum atoms or solvent molecules, but with no chemical meaning.

Results and Discussion

Synthesis and Characterization: As is shown in scheme 1, the reaction of $[Pt(C{\equiv}CR)_4]^{2-}$ with cadmium perchlorate depends on the R substituent. Thus, treatment of the tolyl- and *p*-methoxyphenyl-alkynyl platinum(II) derivatives with Cd^{+2} in acetone leads to the formation of solvate complexes of stoichiometry $[Pt(C{\equiv}CR)_4Cd(acetone)]_2$ **1a,b(acetone)$_2$** (R = Tol **a**, C_6H_4OMe-4 **b**) as bright yellow solids. By contrast, a similar reaction starting from $(NBu_4)_2[Pt(C{\equiv}CC_6H_4OMe\text{-}3)_4]$ results in the precipitation of a solvent-free species $[Pt(C{\equiv}CC_6H_4OMe\text{-}3)_4Cd]_x$ **1'c** as a white solid. The presence of acetone molecules in the former **1a,b(acetone)$_2$** is confirmed by spectroscopic (^{1}H NMR, IR) and analytical data. The proton spectra of freshly prepared $CDCl_3$ solutions reveal the presence of one set of C_6H_4X-4 (X = Me, OMe) and acetone (δ 2.17 ppm) resonances in the ratio 4:1, indicating that all alkynyl groups are equivalent on the NMR

time scale. However, in solid state their IR spectra show several ν(C≡C) bands (2120, 2078 (sh); 2057, 2025 (sh) R = Tol **a**; 2095 (sh), 2057, 2018 (sh) cm^{-1} R = C_6H_4OMe-4 **b**), consistent with the presence of different alkynyl coordination modes. In fact, this pattern is comparable to that observed for the tetranuclear discrete pyridine (**2-4**) and pyrazol (**5**) derivatives, suggesting a similar structure. We have tried to grow crystals of these solvates repeatedly, but all attempts were unsuccessfully. In solid state, we suggest for these solvates a tetranuclear sandwich structure $[Pt(C{\equiv}CR)_4Cd(acetone)]_2$ **1a,b(acetone)$_2$** (Tol **a**, C_6H_4OMe-4 **b**), similar to those found for the solvate **1c(dmso)$_2$** and complexes **2-5,** in which the solvent molecules are bonded to the cadmium center (see Scheme 1). Interestingly, upon prolonged vacuum at ca. 60-70ºC (48 h. **1a(acetone)$_2$**; 3h **1b(acetone)$_2$**), the acetone molecules are removed turning the color from yellow to ochre-orange and the luminescence (under U.V. lamp) from green to weak-orange. The process is reversible and, upon treatment with drops of acetone, the orange luminescence reverts to the yellow-green original (Figure S1). By exploring their solubility in different solvents, we observe that both yellow complexes **1a,b(acetone)$_2$** dissolve in chlorinated solvents such as CH_2Cl_2 or $CHCl_3$, yielding an initial yellow solution. However, in solution these species were found to be unstable, evolving to free-acetone species $[Pt(C{\equiv}CR)_4Cd]_x$ (R = Tol **1'a**; R = C_6H_4OMe-4 **1'b**), which are similar to **1'c** and gradually precipitate (~ 15 min) as white powders. All attempts to obtain crystals of these free-solvent species failed. The most significant and distinctive spectroscopic feature of the **1'a-c** species is observed in their IR spectra, which exhibit one ν(C≡C) band (with a shoulder in **1'a** and **1'b**) in the typical range of η^2-alkynyl bridging ligands (2055, 2023 (sh) cm^{-1} **1'a**; 2055, 2029 (sh) cm^{-1} **1'b**; 2040 cm^{-1} **1'c**). This spectroscopic feature, together with their white color and null solubility in common polar and/or weak donor organic solvents (CH_2Cl_2, $CHCl_3$, CH_3COCH_3,

THF, NCMe), suggest that they are presumably of polymeric nature. It is likely that, in the final free-acetone species **1'a-c**, the Cd^{II} ions shift towards an "*in-plane*" bis-(η^2-alkyne) tweezer like coordination, in such a way that each platinate fragment acts as bis-(chelating) bridging ligand between consecutive cadmium centers. The stabilization of a naked Cd^{II} ion by four η^2 alkynyl ligands has been recently found in the trinuclear anions $[\{(R_f)_2Pt(\mu\text{-}C{\equiv}CR)_2\}_2Cd]^{2-}$ ($R_f = C_6F_5$, R = Bu^t, Ph, Tol).[29] Curiously complexes **1'a-c** proved to be only slightly soluble in d_6-dimethylsulphoxide, allowing their characterization by ^1H NMR spectroscopy (see Experimental). However, in this strong donor solvent the color of the white solids change to yellow, and the small amount that is dissolved (with sonication) yielded deep-yellow solutions, thus indicating that the $(CH_3)_2SO$ molecules presumably interact with the cadmium centers stabilizing tetranuclear species $[Pt(C{\equiv}CR)_4Cd(dmso)]_2$ analogous to complexes **2-5**. Fortunately, after many attempts a few yellow crystals suitable for X-ray could be obtained by slow diffusion of Et_2O into a saturated dmso/CH_2Cl_2 solution of **1'c**, confirming the formation of the solvate $[Pt(C{\equiv}CC_6H_4OMe\text{-}3)_4Cd(dmso)]_2$ **1c(dmso)$_2$** (see below, Figure 4). Tetranuclear aggregates $[Pt(C{\equiv}CR)_4CdL]_2$ (L = py; R = Tol **2a**, C_6H_4OMe-4 **2b**, C_6H_4OMe-3 **2c**. R = Tol; L = $NC_5H_4CH_3$-4 **3**, $NC_5H_4CF_3$-4 **4**, $N_2C_3H_4$ (pzH) **5**) were easily synthesized by treatment of either the acetone solvate **1a,b(acetone)$_2$** or the polymeric **1'a-c** species with the corresponding N-donor ligand. It is worth noting that the same products are obtained even using a large excess of the corresponding ligand, indicating the strong bonding preference of Cd^{II} for the platinum alkyne fragments. The complexes were isolated in moderate (44% **4**, 55% **2c**) or high (75-93% **2a**-**5**) yields as yellow crystals (**2a**, **2c**, **4**, **5**) or microcrystalline yellow powder (**2b**, **3**), and their identities were confirmed by microanalysis and spectroscopic means. The IR spectra of **2a**,**b**, **3-5** show several ν(C≡C) stretching bands in the 2115-2069 cm^{-1} range, in

agreement with the presence of terminal and different asymmetric bridging ligands, as has been confirmed by X-ray crystallography for complexes **2a**, **4** and **5**. For **2c** only one ν(C≡C) stretching band is found (2086 cm^{-1}), being this fact consistent with the presence of only one type of bridging alkynyl ligand, as observed on its X-ray structure. Perspective views of the molecular structures of tolylacetylide derivatives **2a**, **4** and **5** are represented in Figures 1, S2 and 2, respectively, whereas those of the *m*-methoxyphenylacetylide complexes **2c** and the solvate **1c(dmso)$_2$** are shown in Figures 3 and 4. Selected bond lengths and angles are listed in Table 2. As can be seen, the molecules can be visualized as 2:2 adducts giving rise to final rhombohedral Pt_2Cd_2 cores, which are very *asymmetrical* in the tolyl complexes (**2a**, **4**, **5**) and *symmetrical* in the *m*-methoxy derivatives **2c** and **1c(dmso)$_2$**. In any case, one of the most striking features is the fact that, in spite of the relative hard nature of the acidic Cd^{II} ion and the presence of excess of ligand, it only forms one Cd-N(imine) bond (2.239(3) Å **2a**; 2.245(4) **2c**; 2.277(3) **4**; 2.221(4) **5**). Similarly, in the solvate **1c(dmso)$_2$** the Cd is bonded to the oxygen atom of one dimethylsulphoxide molecule with a typical[48] bond distance of 2.224(6) Å. Curiously, in the tolylacetylide aggregates **2a**, **4** and **5** the Cd center of the resulting formed dicationic unit CdL^{+2} forms a very short Pt→Cd donor acceptor bond with the corresponding tetraalkynyl platinate. In fact, the Pt(1´)-Cd(1) bond length (2.6999(3) Å **2a**; 2.7460(3) Å **4**; 2.6952(4) Å **5**) is shorter than the sum of the covalent radii (1.36 (Pt) + 1.44 (Cd) = 2.8 Å)[49] and lies in lower range of reported Pt^{II}-Cd^{II} bond distances, being shorter to that found in [*cis*-$Pt(C_6F_5)_2(C{\equiv}CPh)_2Cd(cyclen)]$ (2.764(1) Å)[39] and close to the shortest one reported to date by Ito et al.[50] in the cation $[(Phpy)_2PtCd(cyclen)]^{+2}$ (2.6389(8) Å, Phpy = 2-phenylpyridinate). Although this fact points to the presence of a significant donation of the electron density from the dz^2(Pt) orbital to the Cd^{II} cation, the Pt-Cd vector displaces

from the normal to the platinate fragment (27.96º **2a**; 32.01º **4**; 26.94º **5**) towards one of the platinum-alkynyl units (Pt-C19-C20), also allowing a close Cd-C$^{\alpha'}$ contact (Cd-C19´ 2.491(4) Å **2a**; 2.475(5) Å **4**; Cd-C19 2.495(5) Å **5**). The resulting neutral {Pt(C≡CR)$_4$CdL} unit dimerizes by rather asymmetrical η^2 interactions of the Cd^{II} with two mutually *cis* alkynyl fragment of the other unit, thus completing a distorted tetrahedral coordination around the Cd^{II} (See Figure S2c for **4**). The observed Cd alkynyl interactions take place mainly with the C$^{\alpha}$ carbon atoms, with Cd-C$^{\alpha}$ distances in the range 2.409(4) to 2.451(4) Å. The Cd-C$^{\beta}$ separations (2.644(4)-2.736(4) Å) are remarkably longer (0.22-0.32 Å) and only close to the sum of the van der Waals radii (2.7 Å) of C^{sp} (1.78 Å)[51] and the ionic radii of Cd^{II} (c.n 4, 0.92 Å),[52] suggesting that the interaction with these atoms is very weak. Notwithstanding, to accommodate these weak Cd···C$^{\beta}$ bonding interactions the platinate units are displaced each other (ca 1.33 Å **2a**; 1.85 Å **4**; 1.97 Å **5**), retaining an eclipsed disposition in **2a** and **5** or with a slight twisting (~ 14º) in complex **4** (see Figure S2). As a consequence of this relative orientation, the interaction of the Cd center with the platinum of the second platinate fragment is remarkably weaker (Pt(1)-Cd(1) 3.1186(3) Å **2a**; 3.0872(3) Å **4**; 3.1289(8) **5**), though still below the Van der Waals limit (3.33 Å).[52] The resulting asymmetrical rhombohedral metallic Pt$_2$Cd$_2$ array is planar in **2a** and **5** and slightly distorted in the *p*-trifluoromethylpyridine derivative **4** (torsion angle 10.58º), with relatively long Pt···Pt (4.2525(2) Å **2a**; 4.0360(2) Å **4**; 4.3017(3) Å **5**) and Cd···Cd (3.9934(4) Å **2a**; 4.1948(4) Å **4**; 3.9503(6) Å **5**) separations. Curiously in **2a** and **5** the corresponding pyridine and pyrazol planes are nearly contained in the metallic plane (small dihedral angles of 18.56º **2a** and 18.64º **5**). In complex **4,** and probably due to the low basicity of the NC$_5$H$_4$CF$_3$-4 relative to py or pzH ligands, the pyridine plane is twisted by 38.35º and the Cd-N vector is also slightly tilded in relation to the plane of the N-donor ligand

(see Figure S2a, ~ 15º in **4** *vs* 2.8º and 4.7º in **2a** and **5,** respectively). As far as the bonding mode of the alkynyl ligands is concerned, it has to be said that, in agreement with the IR spectra, there are two ligands (C(28)-C(29)-Tol) that remain as terminal groups (one from each platinate unit), two acting as μ-κ^2C$^\alpha$ bridging ligands and the remaining four that exhibit a rather unsymmetrical μ-κ^2C$^\alpha$:η^2 bridging mode. Despite this dissimilarity no clear correlation can be found between the bonding mode and their structural details (see Table 2).

The pyrazol derivative **5** crystallizes in the P-1 space group with one molecule of acetone in the asymmetrical unit, which oxygen atom (O1) is involved in intermolecular hydrogen bonds with the N-H hydrogen atom of the corresponding pyrazol groups (Figure 2). The H(2)···O(1) and N(2)···O(1) distances (2.197 and 2.860 Å respectively) and the N(2)-H(2)-O(1) angle (133.76º) are within the usual range for this type of contacts.[53-57]

The structures of the *m*-metoxyalkynyl derivatives **2c** and **1c(dmso)$_2$** (Figures 3 and 4, respectively) display a symmetrical framework in which the two tetraalkynyl platinates are eclipsed, and both cationic cadmium units symmetrically bisect the alkynyl entities, being bonded to four Pt-C$^\alpha$ bonds (two associated with each platinum unit). As a consequence, in both derivatives the alkynyl ligands display a μ-κ^2C$^\alpha$ bonding mode and the Cd^{II} ion is in an approximately square pyramidal geometry, with the midpoint of the four Pt-C$^\alpha$ bonds occupying the basal plane, and the pyridine (**2c**) or the dmso (**1c(dmso)$_2$**) at the apex. As expected, the Cd-C$^\alpha$ distances (range 2.471(5)-2.551(5) Å **2c**; 2.470(10)-2.508(10) Å **1c(dmso)$_2$**) are comparable to those found for the μ-κ^2C$^\alpha$ bridging ligand in the tolyl-acetylide derivatives (2.475(5)-2.495(5) Å). In the final rombohedric planar $Pt_2Cd_2E_2$ (E = N, O) cores, the four Pt→Cd bonds are now nearly symmetrical (Pt-Cd 2.8001(4), 2.8505(4) Å **2c**; 2.9052(8), 2.914(8) Å **1c(dmso)$_2$**). The

value of the medium Pt-Cd separation in the pyridine complex **2c** (~ 2.825 Å) is only somewhat shorter than the corresponding averages values between the shortest and the longest Pt-Cd distances found in the unsymmetrical tolylderivatives (averages 2.9092 Å **2a**; 2.9166 Å **4**; 2.9121 Å **5**), suggesting that the stabilization of these clusters involve a synergistic combination of Pt···Cd, Cd···alkynyl and Cd-N bonding interactions. Although it is not clear which is the reason by what symmetrical aggregates are not favored in the tolyl derivatives, it seems likely that the preferred formation of a very short Pt→Cd bond in **2a**, **4** and **5** is responsible of the absence of interaction of the Cd^{II} with one of the alkynyl ligands. A similar structural feature was found in the bimetallic [*cis*-$Pt(C_6F_5)_2(C{\equiv}CPh)_2Cd(cyclen)$], in which the Cd is bonded to platinum (Pt-Cd 2.775(1) Å) and contacts only with one of the C^{α} carbon atoms.[39] In **2c** and **1c(dmso)$_2$**, the presence of OMe substituents favors the existence of weak intermolecular non-covalent interactions, leading to the generation of a complex supramolecular network (see S3 as illustration for **2c**).

Complex **2b** is only soluble in d^6-dmso, but in this strong donor solvent the recorded ^1H NMR pattern reveals the presence of free pyridine (8.58 (d); 7.78 (t); 7.38 (dd)) and an identical AB pattern (δ 7.20 and 6.82, J = 8.6 Hz) for the aryl C_6H_4OMe-4 protons to that seen for the precursor **1'b** in d^6-dmso, suggesting that similar [$Pt(C{\equiv}CC_6H_4OMe\text{-}4)_4Cd(dmso)]_2$ species are present in this solvent. In contrast, complexes **2a,c** and **3** dissolves in CD_2Cl_2 (**2c**) or $CDCl_3$ (**2a**, **3**) and both the *low* field shifts of the pyridine *ortho* protons ($\Delta H^{2,6}$ = 0.46 **2a**; 0.27 ppm **2c**, **3**) and the pattern of the aryl C_6H_4R protons, shifted to low frequencies respect to $[Pt(C{\equiv}CC_6H_4R)_4]^{2-}$, support that the integrity of the tetranuclear aggregates remains in solution. The lower basicity of the $NC_5H_4CF_3$-4 ligand is reflected in the behavior of complex **4** in solution. Thus, its proton spectrum ($CDCl_3$) shows the presence of an equilibrium mixture of the precursor

1a and complex **4** (δ 6.88, 6.65; AB system C_6H_4Me-4) in a ca. molar ratio 3:2. To investigate this behavior, the proton spectra of **1a** were recorded in the presence of increased amounts of $NC_5H_4CF_3$-4. As shown in Figure S4, upon addition of 2 equivalents of $NC_5H_4CF_3$-4, the observed pattern is identical to that obtained with crystals of complex **4**. Upon progressive addition of ligand, the resonances of **1a** gradually decrease, whereas those of complex **4** increase, being necessary a large excess of pyridine (6 equiv.) to move completely the equilibrium towards complex **4**. The presence of only one set of pyridine protons (δ 8.87 $H^{2,6}$; 7.42 $H^{3,5}$), very close to those of free $NC_5H_4CF_3$-4 (δ 8.81 $H^{2,6}$; 7.51 $H^{3,5}$), supports its involvement in a fast additional exchange with complex **4**. The ^{195}Pt NMR spectrum of a $CDCl_3$ solution containing **4** and $NC_5H_4CF_3$-4 (1:4 molar ratio) could be recorded (Figure 5), showing the presence of a singlet at -3761 ppm with both ^{111}Cd ($^1J(^{195}Pt\text{-}^{111}Cd)$ = 1855 Hz) and ^{113}Cd ($^1J(^{195}Pt\text{-}^{113}Cd)$ = 1941 Hz) satellites. The observed relative ratio 1:3:1 matches that expected for a tetranuclear Pt_2Cd_2 aggregate, ruling out the formation of binuclear Pt-Cd units (expected ratio 1:4:1) in the presence of excess of pyridine. We are not aware of previously reported one bond $^{195}Pt\text{-}^{111,113}Cd$ coupling constants.[50,58,59] In **4**, both the remarkable downfield of the platinum resonance in relation to the anionic precursor $(NBu_4)_2[Pt(C{\equiv}CTol)_4]$ (δ -4187 ppm) and the high value of the Pt-Cd coupling constants are indicative of a relative strong Pt→Cd dative bond.

The ^{1}H NMR spectrum of the pyrazol derivative **5** in CD_2Cl_2 exhibits, in addition to the aromatic tolyl protons, two characteristic resonances at δ 11.97 (br) and at 6.27 ppm (pt, J = 2.4 Hz) due to H^1 and H^4 protons, but only a broad signal (~ 7.34 ppm) for H^3 and H^5, indicating that they are involved in a dynamic process. Upon cooling, coalescence is observed at ca 293 K and, finally, the resonance split into two discrete signals (δ 7.50 and 7.17 ppm). The calculated energy barrier for the interconversion of H^3 and H^5

protons at the coalescence temperature is $\Delta G_{293}^{\#}$ ~ 58.43 KJ·mol^{-1}. Addition of slight excess of pzH to this solution at r.t. only causes a significative sharpening of the $H^{3,5}$ resonance and a slight upfield shift for H^1 (δ 11.78 ppm), thus suggesting that a fast dissociative ligand process would be responsible for the observed average of H^3 and H^5 protons in this complex.

Photophysical characterization

Absorption spectroscopy: The absorption data for all the complexes are summarized in Table S1. In solid state, the diffuse-reflectance of the yellow tetranuclear aggregates are characterized by a distinctive low energy feature in the range 370 for **2c** to 385 nm for **2b** with a long tail to ~ 475 nm, which is absent in the white solvent free **1'a-c** derivatives. As illustration, the spectra of the free **1'c** and solvate **1c(dmso)$_2$** and the pyridine adducts **2a-c** are given in Figure S5 and S6, respectively.

As mentioned above, the solvate **1a,b(acetone)$_2$** $[Pt(C{\equiv}CR)_4Cd(acetone)]_2$, are only soluble in chlorinate solvents, in which they are unstable evolving to solvent free insoluble derivatives **1'a-c**. The spectra of *freshly* prepared CH_2Cl_2 solutions of both complexes (see Figure S7 for **1b(acetone)$_2$**) show several high energy features (200-266 nm, see Table S1) due to intraligand transitions and a low energy absorption (316 nm **1a(acetone)$_2$**; 319 nm **1b(acetone)$_2$**), which appear remarkably blue shifted in relation to the lowest $^1\pi\pi$ IL/dπ(Pt)$\rightarrow\pi^*$(C≡CR) MLCT manifold in the corresponding precursors $[Pt(C{\equiv}CR)_4]^{2-}$ (CH_2Cl_2; 335, 345*sh* R = Tol; 344 R = C_6H_4OMe-4). Similar hypsochromic shifts have been previously observed in tweezer-like heterometallic Pt-Cd complexes, being attributed to the existence of a lesser electronic dπ(Pt)/C≡C interaction caused by the *in-plane* η^2-Cd complexation, which probably lowers the energy of the alkynyl based HOMO.[29] The shift to higher energies observed for

1a,b(acetone)$_2$ in the low energy band suggest that, in CH_2Cl_2 solution, the acetone molecules are likely lost and the Cd^{II} centers probably move towards an in-plane η^2-coordination with the alkynyl ligands. Interestingly, the progressive addition of acetone to the CH_2Cl_2 solution causes the growth of a new low energy-band at ca. 372 nm for **1a(acetone)$_2$** and at 377 nm in **1b(acetone)$_2$** (see Figure S7 for **1b(acetone)$_2$**). The position of these bands compares to those observed for the tetranuclear aggregates **2-5**, being suggestive of the coordination of the acetone molecules to cadmium centers, with the concomitant formation of the solvate $[Pt(C{\equiv}CR)_4Cd(acetone)]_2$ species in solution to some extent. Only in the presence of excess of dmso (mixture CH_2Cl_2:dmso 9:1) the spectrum of **1c(dmso)$_2$** shows two low energy bands (348 and 371 nm), and a similar pattern to that observed for the pyridine clusters (345, 377 nm **2a**, 348, 375 nm **2c** and 348, 376 nm **3**), which seems to be characteristic of the tetranuclear cluster entities $[Pt_2(C{\equiv}CR)_8Cd_2L_2]$ (Figure 6). In the same line, the existence of a remarkable dissociation of the $NC_5H_4CF_3$-4 ligand for **4**, was also confirmed by UV-Vis spectroscopy. As illustration, Figure 7 shows the spectra of the precursor **1a(acetone)$_2$** and the microcrystalline solid **4,** together with the changes observed upon the addition of $NC_5H_4CF_3$-4. The band at ~ 316 nm, which resembles the ^{1}IL/MLCT band of the precursor, is progressively depleted, while the band at 376 nm due to **4** grows and a shoulder at 348 nm, typical of the tetranuclear aggregates, is also clearly seen when more than 10 eq. of $NC_5H_4CF_3$-4 are added. The presence of a clear isosbestic point indicates that a simple equilibrium between **1a** and **4** is involved.

The two distinctive low energy absorptions exhibit only a small dependence with the alkynyl substituents and the coligands at cadmium. An slight blue shift is observed from **2a** (Tol, py) to **2c** (C_6H_4OMe-3, py) and, in the tolyl derivatives, the energy follows the order **5** (367 nm) > **1a(acetone)$_2$** (372 nm) > **2a** (377 nm) ~ **3** (377 nm) ~ **4** (376 nm).

Following previous assignments,[24,30,34,38] these absorptions are attributed to an admixture of Pt/π(C≡CR)→π*(C≡CR) (MLCT) and platinum-ligand to cadmium charge transfer Pt(C≡CR)→Cd. Alternatively, we denoted the transition as MLM´CT (M = Pt, M´ = Cd) with intraligand character. Although the influence of coligands at Cd is less obvious, it seems that the coordination to pyridine ligands causes a slight red shift in the absorption maxima, most likely due to the occurrence of some mixing with platina-alkynyl to pyridine charge transfer character MLL´CT, as suggested by TD-DFT calculations.

Emission spectroscopy: All tetranuclear aggregates **1a,b(acetone)$_2$**, **1c(dmso)$_2$**, **2-5** are strongly emissive in the solid state (298, 77 K), with high quantum yields in the range 4.5 - 36.3 % for the nitrogen coordinated derivatives **2-5** (Table 3). These latter also exhibit moderate luminescence in CH_2Cl_2 solution at 298 K. The calculated emission lifetimes fit to monoexponential decays in the range of microseconds, revealing their triplet state parentage. Figure 8 shows the emission spectra of the yellow solvate complexes in solid state at 298 and 77 K. They exhibit a bright greenish luminescence (488 nm **1a(acetone)$_2$**, 515 nm **1b(acetone)$_2$**, 500 nm **1c(dmso)$_2$**), which is blue-shifted and slightly structured at 77 K (λ_{max} 484 nm **1a(acetone)$_2$**, 489 nm **1b(acetone)$_2$**, 492 nm **1c(dmso)$_2$**), pointing to the involvement of the alkynyl ligands in the excited state. The emission occurs at lower energies compared with that of the anionic precursors,[40] and decreases (Tol > C_6H_4OMe-3 > C_6H_4OMe-4) with the electron donating ability of the alkynyl groups, indicating that they must be involved in the lowest excited state. We assign the emission in these solvates as platinum-alkynyl to cadmium charge transfer ^{3}MLM´CT (Pt(d)/π(C≡CR)→Pt(P_z)Cd(s)/π*(C≡CR)) mixed with some intraligand character (^{3}IL C≡CR), as supported from the DFT studies (*vide infra*). As commented above, after prolonged vacuum the solvate derivatives **1a,b(acetone)$_2$** lost the acetone

molecules affording final ochre-orange solids, which are weakly emissive displaying broader red-shifted emission bands centered at ca. 510 nm (**1a**) and 560 nm (**1b**), respectively (see Figure S8 for **1a**). The process is reversible for several cycles (at least 4), and the initial yellow colors and green luminescence are recovered upon exposure of the orange solids to a drop of acetone (see Figure S1). We think that the lost of acetone probably takes place with retention of the sandwich type structure. The change in color and the observed bathochromic shift in the emissions could be ascribed to the existence of stronger out of plane alkynyl-η^2-cadmium bonding interactions in **1a**,**b** in relation to the solvates, which presumably lower the energy of the π*(C≡CAryl) fragments, reducing the gap of the transition. The white free solvent-insoluble materials **1'(a-c)** are, however, only weakly emissive at low temperature (see Table 3).

Microcrystalline solids **2**-**5** display (Figure 9, solid lines) structureless emission bands in the range 488 to 545 nm at room temperature, which are blue shifted at 77 K (469-530 nm see Table 3). Interestingly, the emission band of these complexes is significantly red-shifted in CH_2Cl_2 solution (Figure 9, dotted lines) from those in solid state; being the extent of the red-shifts in solution (1646 **2a**, 1385 **2c**; 1695 **3**; 1487 **4** and 712 cm^{-1} **5**) comparable to those previously observed in other heteropolynuclear Pt_2M_4 (M = Cu, Ag, Au) complexes.[38,60] This behavior, denoted as rigidochromism, has been attributed to structural changes in the excited state, which are more favorable in solution than in the rigid lattice of the solid.[61] It should be noted that the excitation spectra in solution resemble the corresponding absorption spectra, suggesting that the emission comes from the tetranuclear $\{Pt_2(C{\equiv}CR)_8Cd_2L_2\}$ aggregates (see figure S9 for complex **3**). As can be seen in Figure 9, the emission energy was found to change upon variation of both the alkynyl ligand and the N-donor ligand at cadmium. This latter has a prominent effect on the emission energy following the same trend in solid state (488 **3**

> 490 **2a** > 505 **4** > 545 nm **5**) than in solution (532 **3** > 533 **2a** > 546 **4** > 567 nm **5**), which is in line with the electron-accepting ability of the N-imine ligand ($NC_5H_4CH_3$-4 < NC_5H_5 <$NC_5H_4CF_3$-4 < pzH). Also, both at 298 and at 77 K, the emission energy of **2b** (520 nm 298 K; 500 nm 77 K) is red-shifted in relation to **2c** (492 nm 298 K; 469 nm 77 K) and **2a** (490 nm 298 K; 479 nm 77 K). This fact reflects the role of the better electron delocalization between the C≡C and aryl in the *p*-methoxy phenylethyl fragment, which reduces the gap of the transition. Taken into account these trends and the salient features of the frontier orbitals (see below), which indicate the role of the pyridine ligands in the lowest unoccupied orbitals LUMO and L+1 for complexes **2a**, **2c** and **4**, we suggest that the emission comes from an excited state of large Pt(d)/π(C≡CR)→π*(imine) MLL´CT character, mixed with Pt(d)π(C≡CR)→Pt_2Cd_2/π*(C≡CR) (MLM´CT) contribution. Upon cooling to 77 K the CH_2Cl_2 solutions, the emission bands remarkably shift to higher energies exhibiting profiles somewhat structured (see Figure S10) with λ_{max} at 460 **2a** ~ 450 (**3**, **4**) and 496 nm **5**. Although less structured, the emissions of **2a**, **3** and **4** resemble to that found in $(NBu_4)_2[Pt(C{\equiv}CTol)_4]$ (λ_{max} 456, 480, 502, 530 nm),[40] suggesting that in frozen CH_2Cl_2 their emissions could be ascribed to a ^{3}IL(ππ*)/^{3}MLCT manifolds of the platinate fragments. For **5** the emission is broader and red-shifted in relation to $[Pt(C{\equiv}CTol)_4]^{2-}$, making clear the influence of the "Cd(pzH)" units.

Molecular orbitals calculations: Density Functional Theory (DFT) calculations are currently used to stablish the electronic structure and spectral transitions. In this work, single point (DFT) and time-dependent (TD-DFT) Density Functional Calculations were performed for **1c(dmso)$_2$**, **2a,c**, **4** and **5**. Table 4 summarizes the orbital compositions for all five complexes in terms of ligands and metals. As can be seen, the calculations reveal some differences between the pyridine-cadmium coordinated

aggregates (**2a,c**, **4**) and complexes **1c(dmso)$_2$** and **5**. The three pyridine complexes **2a,c** and **4** have similar frontier orbitals, those of **2a** are shown in Figure 10, and those of **2c** and **4** in Supporting Information (Figure S11). In these complexes, the last higher occupied molecular orbitals possess a strong alkynyl and platinum character. Thus, the HOMO and H-1 comes from the combination of the Pt(II) dπ orbitals (~ 15 %) with two mutually *trans* π(C≡CAryl) (83-86 %) alkynyl ligands on each platinate fragment, and the H-2 and H-3 are similar, but building up from the other mutually *trans* alkynyl ligands. The LUMO and L+1 are composed mainly of the π* of the pyridine ligands (97% **2a**; 91% **2c**; 98% **4**) with a negligible contribution of metals (Cd ~ 1%) and alkynyl fragments. However, the L+2, which is ~ 0.43 (**2a**), 0.34 (**2c**) and 0.79 eV (**4**) higher than the LUMO, has alkynyl (54-60 %) and remarkable Pt_2Cd_2 metallic (Pt(p) 25-29 % / Cd(s) 10-13 %) character. As can be seen in Table 4, (see also Figures 10 and S11), for complexes **1c(dmso)$_2$** and **5** the composition of the HOMOs (H-3 to HOMO) is essentially similar to those for **2a,c** and **4,** being composed of platinum and alkynyl ligands. However, in these derivatives there is a major difference in the unoccupied orbitals, because now the LUMO and L+1 are metal and alkynyl ligand based. Thus, for both 1c(dmso)2 and 5 the LUMO is a cluster localized Pt_2Cd_2 metallic orbital (Pt (22-29 %), mainly P_z; Cd (11-13 %) mainly s), which exhibits σ Cd-Cd bonding character with remarkably alkynyl contribution (67, 58 %). In the L+1 the contribution of cadmium in both complexes is similar to that of LUMO, while that of Pt(II) is lower. The difference between **1c(dmso)$_2$** and **5** is observed in the following unoccupied orbitals. In **1c(dmso)$_2$** the L+2 and L+3 have preponderant alkynyl contribution while in the pyrazol derivative **5** the L+2 is composed of 90 % of pzH, and the L+3 contains contribution from pzH (69 %) and C≡CTol (25 %).

The nature of the absorption features were explored by TD-DFT calculations using the polarized continuum model in which the solvent is simulated at a continuum of uniform dielectric constant. Calculated transitions energies in CH_2Cl_2 solutions (first singlets) with strong oscillator strengths, which have higher contribution to the absorption spectra, are summarized in Table S2. For complex **1c(dmso)$_2$**, the lowest-energy absorptions (HOMO-n to LUMO) involve transitions from platinum-alkynyl orbitals based (PtC≡CR) to the LUMO, a (Pt_2Cd_2)/π*C≡CR orbital, which can be assigned as MLM´CT (M = Pt, M´ = Cd) platinum-alkynyl-to-cadmium charge transfer. The calculated values (353, 346, 331 nm) can be related with experimental values seen in CH_2Cl_2 (371, 348*sh* nm) (Figure 6). A similar assignment can be made for complex **5**. In this complex, the three lowest computed absorptions are calculated at 380, 356 and 351 nm, resulting mainly from HOMO→LUMO, H-3→LUMO and H-1→L+1, respectively. Experimentally, the lowest band is located at 367 nm, exhibiting a long tail spreading down to ~ 430 nm. In the pyridine derivatives the lowest energy absorptions calculated (348-369 nm **2a**; 345-370 nm **2c**; 329-395 nm **4**) correspond to the excitations from HOMO-n to LUMO, L+1 and L+2 (see Table S1). Therefore, as the LUMO and L+1 are π* orbitals localized in the pyridine ligands and L+2 is Pt_2Cd_2/π*C≡CR based in these aggregates, the two low energy absorptions can be assigned as admixture of PtC≡CR→π*(pyridine) (MLL´CT) and MLM´CT. This involves charge transfer from the platina-alkynyl fragments towards the pyridine ligand, mainly in the lowest feature for **2a,c** (Figure 6), but also to the metallic core and π*C≡CR (Pt_2Cd_2/π*C≡CR).

Conclusions.

In summary, depending on the solvent and the alkynyl substituent (R = Tol **a**, C_6H_4OMe-4 **b**, C_6H_4OMe-3 **c**), Cd^{2+} coordinates to the anionic homoleptic substrates $[Pt(C{\equiv}CR)_4]^{2-}$ to yield yellow sandwich-type tetranuclear solvate complexes $[Pt(C{\equiv}CR)_4Cd(solvent)]_2$ (**1a,b(acetone)$_2$**, **1c(dmso)$_2$** (X-ray)) or white polymeric free solvate species $[Pt(C{\equiv}CR)_4Cd]_x$ **1'a-c**. In the solid state, the solvates **1a,b(acetone)$_2$**, which exhibit a bright green luminescence (488 **a**, 515 nm **b**), lost reversibly the acetone molecules affording ochre-orange solids with a very weak red-shifted emission (~ 510 **1a**, 560 **1b**). However, in chlorinate solvents they are not stable, evolving to insoluble **1'a-c**. Addition of N-donors ligands results in the formation of very stable **2-5** tetranuclear complexes, in which two dicationic CdL^{2+} units are stabilized by synergistic combination of Pt···Cd and Cd···alkynyl bonding interactions, as confirmed by X-ray diffraction and spectroscopic studies. Two type of planar rhombohedral Pt_2Cd_2 frameworks are found. Asymetrical with two very short (~ 2.7 Å) and two weaker (~ 3.1 Å) Pt···Cd bonding interactions in the tolyl derivatives (**2a**, **4** and **5**) and symmetrical, stabilized with four similar Pt···Cd interactions (~ 2.85 Å), in the meta-methoxyphenylalkynyl derivatives **1c(dmso)$_2$** and **2c**. As a consequence, the former exhibit three different alkyny ligation modes (μ-η^2, μ-κC^α and σ-C≡CR), while in **1c(dmso)$_2$** and **2c** all alkynyls adopt a μ-κC^α bonding mode. In addition, **2-5** are highly phosphorescent both in solid state (Φ from 4,5 to 36.3 %) and in solution, with emission maxima depending on the alkynyl substituent and the coligand. Both the experimental data and TD-DFT calculations suggest that excitation of these clusters moves electron density from both platina-alkynyl fragments towards low-lying orbitals, which have strong metallic/alkynyl (Pt_2Cd_2/π*C≡CR) character in the case of the solvate and pyrazol (**5**) derivatives or a remarkable contribution of the π* pyridine groups in the

pyridine derivatives **2**-**4**. All these properties may be useful in potential practical applications.

Acknowledgment. We thank the Spanish MICINN for financial support (Projects CTQ2008-06669-C02-01, 02). J. Fernández thanks the CAR and S. Sanchez to the CSIC for a grant. We also thank CESGA for computer support.

Supporting Information Available: This material is available free of charge via the Internet at http://pubs.acs.org: Complete details concerning the synthesis and spectroscopic characterization of the complexes **1**-**5**. Computational details for DFT calculations. Diffuse reflectance and absorption data for complexes **1**-**5** in solid state and solution respectively (Table S1). Calculated transition energies in CH_2Cl_2 solutions for **1c(dmso)$_2$**, **2a**, **2c**, **4** and **5** (Table S2). Photographic images under white and UV light of **1a(acetone)$_2$** and its reversible transformation into **1a** (Figure S1). ORTEP views of complex **4** (Figure S2). Supramolecular details and views of the tridimensional organization of complex **2c** (Figure S3). ^{1}H NMR of a $CDCl_3$ solution of **1a** upon progressives additions of $NC_5H_4CF_3$-4 (Figure S4). Solid diffuse reflectance of complexes **1'c**, **1c(dmso)$_2$**, **2a**, **2b** and **2c** (Figures S5 and S6). Absorption spectra of a freshly prepared solution of **1b(acetone)$_2$** in CH_2Cl_2 and in different mixtures of CH_2Cl_2:acetone (Figure S7). Emission spectra of **1a(acetone)$_2$** (solid line) and **1a** (dashed line) in solid state ant 298 K (Figure S8). Absorption and excitation spectra of a CH_2Cl_2 5×10^{-5} M solution of **3** (Figure S9). Emission spectra of CH_2Cl_2 5×10^{-5} M solutions of **2a**, **3**, **4** and **5** at 77 K (Figure S10). Frontier orbital plots for **2c**, **4** and **5** (Figure S11). Crystallographic data in CIF format.

Footnotes

* Corresponding author. E-mail: elena.lalinde@unirioja.es (E. L.).

References

(1) For some reviews see: (a) Nast, R. *Coord. Chem. Rev.* **1982**, *47*, 89. (b) Manna, J.; John, K. D.; Hopkins, M. D. *Adv. Organomet. Chem.* **1995**, *38*, 79. (c) Forniés, J.; Lalinde, E. *A. Perspective. J. Chem. Soc., Dalton Trans.* **1996**, 2587. (d) Belluco, U.; Bertani, R.; Michelin, R. A.; Mozzon, M. *J. Organomet. Chem.* **2000**, *600*, 37. (e) Long, N. J.; Williams, C. K. *Angew. Chem., Int. Ed. Engl.* **2003**, *42*, 2586. (f) Bruce, M. I.; Low, P. J. *Adv. Organomet. Chem* **2004**, *50*, 179. (g) Mak, T. C. W.; Zhao, X.-L.; Wang, Q.-M.; Guo, G.-C. *Coord. Chem Rev* **2007**, *251*, 2311. (h) Mathur, P.; Chatterjee, S.; Avasare, V. D. *Adv. Organomet. Chem* **2008**, *55*, 201. (i) Ren, T. *Organometallics* **2005**, *24*, 4854. (j) Akita, M.; Koike, T. *A. Perspective., Dalton Trans.* **2008**, 3523. (k) Szafert, S.; Gladysz, J. A. *Chem. Rev.* **2003**, *103*, 4175. (l) Nguyen, P.; Gómez-Elipe, P.; Manners, I. *Chem. Rev.* **1999**, *99*, 1515.

(2) Wong, W.-Y. *Coord. Chem Rev* **2007**, *251*, 2400.

(3) Hissler, M.; McGarrah, J. E.; Connick, W. B.; Geiger, D. K.; Cummings, S. D.; Eisenberg, R. *Coord. Chem. Rev.* **2000**, *208*, 115.

(4) Yam, V. W.-W.; Lo, K. K.-W. *Chem. Soc. Rev.* **1999**, *28*, 323.

(5) Yam, V. W.-W.; Lo, K. K.-W.; Wong, K. M.-C. *J. Organomet. Chem.* **1999**, *578*, 3.

(6) Yam, V. W.-W.; Lo, W.-Y.; Lam, C.-H.; Fung, W. K.-M.; Wong, K. M.-C.; Lau, V. C.-Y.; Zhu, N. *Coord. Chem. Rev.* **2003**, *245*, 39.

(7) Yam, V. W.-W. *J. Organomet. Chem.* **2004**, *689*, 1393.

(8) Wong, W.-Y. *A Perspective, Dalton Trans.* **2007**, 4495.

(9) Chen, Z.-N.; Zhao, N.; Fan, Y.; Ni, J. *Coord. Chem Rev* **2009**, *253*, 1.

(10) Castellano, F. N.; Pomestchenko, I. E.; Shikhova, E.; Hua, F.; Muro, M. L.; Rajapakse, N. *Coord. Chem. Rev.* **2006**, *250*, 1819.

(11) Ziessel, R.; Hissler, M.; El-ghayoury, A.; Harriman, A. *Coord. Chem. Rev.* **1998**, *178 -180*, 1251.

(12) For some recent works see: (a) Rios, D.; Olmstead, M. M.; Balch, A. L. *Inorg. Chem.* **2009**, *48*, 5279. (b) Umakoshi, K.; Saito, K.; Arikawa, Y.; Onishi, M.; Ishizaka, S.; Kitamura, N.; Nakao, Y.; Sakaki, S. *Chem. Eur. J* **2009**, *15*, 4238. (c) Yue, C.; Yan, C.; Feng, R.; Wu, M.; Chen, L.; Jiang, F.; Hong, M. *Inorg. Chem., 48*, 2873. (d) Fernández, E. J.; Laguna, A.; López-de-Luzuriaga, J. M. *Dalton Trans.* **2007**, 1969. (e) Forniés, J.; García, A.; Lalinde, E.; Moreno, M. T. *Inorg. Chem.* **2008**, *47*, 3651. (f) Falvello, L. R.; Forniés, J.; Garde, R.; García, A.; Lalinde, E.; Moreno, M. T.; Steiner,

A.; Tomás, M.; Usón, I. *Inorg. Chem.* **2006**, *45*, 2543. (g) Falvello, L. R.; Forniés, J.; Lalinde, E.; Menjón, B.; García-Monforte, M. A.; Moreno, M. T.; Tomás, M. *Chem. Commun.* **2007**, 3838. (h) Yam, V. W.-W.; Cheng, E. C.-C. *Chem. Soc. Rev.* **2008**, *37*, 1806. (i) Balch, A. L. **2007**, *123*, 1. (j) Kato, M. *Bull. Chem. Soc. Jpn.* **2007**, *80*, 287. (k) Katz, M. J.; Michaelis, V. K.; Aguiar, P. M.; Yson, R.; Lu, H.; Kaluarachchi, H.; Batchelor, R. J.; Schreckenbach, G.; Kroeker, S.; Patterson, H. H.; Leznoff, D. B. *Inorg. Chem.* **2008**, *47*, 6353. (l) Katz, M. J.; Ramnial, T.; Yu, H.-Z.; Leznoff, D. B. *J. Am. Chem Soc.* **2008**, *130*, 10662. (m) Elbjeirami, O.; Omary, M. A. *J. Am. Chem Soc.* **2007**, *129*, 11384. (n) Xia, B.-H.; Zhang, H.-X.; Che, C.-M.; Leung, K.-H.; Phillips, D. L.; Zhu, N.; Zhou, Z.-Y. **2003**, *125*, 10362. (o) Gade, L. H. *Angew. Chem. Int. Ed.* **2001**, *40*, 3573.

(13) Eryazici, I.; Moorefield, C. N.; Newkome, G. R. *Chem. Rev.* **2008**, *108*, 1834.

(14) Yam, V. W.-W.; Chan, K. H.-Y.; Wong, K. M.-C.; Zhu, N. *Chem. Eur. J.* **2005**, *11*, 4535.

(15) Koshevoy, I. O.; Lin, Y.-C.; Karttunen, A. J.; Haukka, M.; Chou, P.-T.; Tunik, S. P.; Pakkanen, T. A. *Chem. Commun.* **2009**, 2860.

(16) Wei, Q.-H.; Yin, G.-Q.; Zhang, L.-Y.; Shi, L.-X.; Mao, Z.-W.; Chen, Z.-N. *Inorg. Chem.* **2004**, *43*, 3484.

(17) Koshevoy, I. O.; Karttunen, A. J.; Tunik, S. P.; Haukka, M.; Selivanov, S. I.; Melnikov, A. S.; Serdobintsev, P. Y.; Pakkanen, T. A. *Organometallics* **2009**, *28*, 1369 and ref. therein.

(18) Charmant, J. P. H.; Forniés, J.; Gómez, J.; Lalinde, E.; Merino, R. I.; Moreno, M. T.; Orpen, A. G. *Organometallics* **1999**, *18*, 3353.

(19) Charmant, J. P. H.; Falvello, L. R.; Forniés, J.; Gómez, J.; Lalinde, E.; Moreno, M. T.; Orpen, A. G.; Rueda, A. *Chem. Commun.* **1999**, 2045.

(20) Ara, I.; Forniés, J.; Gómez, J.; Lalinde, E.; Moreno, M. T. *Organometallics* **2000**, *19*, 3137.

(21) Forniés, J.; Gómez, J.; Lalinde, E.; Moreno, M. T. *Inorg. Chem.* **2001**, *40*, 5415.

(22) Berenguer, J. R.; Forniés, J.; Gómez, J.; Lalinde, E.; Moreno, M. T. *Organometallics* **2001**, *20*, 4847.

(23) Berenguer, J. R.; Forniés, J.; Gil, B.; Lalinde, E. *Chem. Eur. J.* **2006**, *12*, 785.

(24) Gil, B.; Forniés, J.; Gómez, J.; Lalinde, E.; Martín, A.; Moreno, M. T. *Inorg. Chem.* **2006**, *45*, 7788.

(25) Yam, V. W.-W.; Hui, C.-K.; Yu, S.-Y.; Zhu, N. *Inorg. Chem.* **2004**, *43*, 812.

(26) Yin, G.-Q.; Wei, Q.-H.; Zhang, L.-Y.; Chen, Z.-N. *Organometallics* **2006**, *25*, 580.

(27) Wei, Q.-H.; Yin, G.-Q.; Ma, Z.; Shi, L.-X.; Chen, Z.-N. *Chem. Commun.* **2003**, 2188.

(28) Yam, V. W.-W.; Yu, K.-L.; Cheung, K.-K. *J. Chem. Soc., Dalton Trans.* **1999**, 2913.

(29) Fernández, J.; Forniés, J.; Gil, B.; Gómez, J.; Lalinde, E.; Moreno, M. T. *Organometallics* **2006**, *25*, 2274.

(30) Berenguer, J. R.; Gil, B.; Fernández, J.; Forniés, J.; Lalinde, E. *Inorg. Chem.* **2009**, *48*, 5250.

(31) Ara, I.; Berenguer, J. R.; Forniés, J.; Gómez, J.; Lalinde, E.; Merino, R. I. *Inorg. Chem.* **1997**, *36*, 6461.

(32) Charmant, J. P. H.; Forniés, J.; Gómez, J.; Lalinde, E.; Merino, R. I.; Moreno, M. T.; Orpen, A. G. *Organometallics* **2003**, *22*, 652.

(33) Ara, I.; Berenguer, J. R.; Eguizábal, E.; Forniés, J.; Gómez, J.; Lalinde, E. *J. Organomet. Chem.* **2003**, *670*, 221.

(34) Berenguer, J. R.; Díez, A.; Fernández, J.; Forniés, J.; García, A.; Gil, B.; Lalinde, E.; Moreno, M. T. *Inorg. Chem.* **2008**, *47*, 7703.

(35) Forniés, J.; Fuertes, S.; Martín, A.; Sicilia, V.; Gil, B.; Lalinde, E. *Dalton Trans.* **2009**, 2224.

(36) Díez, A.; García, A.; Lalinde, E.; Moreno, M. T. *Eur. J. Inorg. Chem.* **2009**, 3060.

(37) Forniés, J.; Gómez, J.; Lalinde, E.; Moreno, M. T. *Inorg. Chim. Acta* **2003**, *347*, 145.

(38) Forniés, J.; Fuertes, S.; Martín, A.; Sicilia, V.; Lalinde, E.; Moreno, M. T. *Chem. Eur. J* **2006**, *12*, 8253.

(39) Forniés, J.; Ibáñez, S.; Martín, A.; Gil, B.; Lalinde, E.; Moreno, M. T. *Organometallics* **2004**, *23*, 3963.

(40) Benito, J.; Berenguer, J. R.; Forniés, J.; Gil, B.; Gómez, J.; Lalinde, E. *Dalton Trans.* **2003**, 4331.

(41) Otwinowski, Z.; Minor, W. *Methods in Enzymology* **1997**, *276*, 307.

(42) Sheldrick, G. M. *SHELX-97, a program for the refinement of crystal structures* University of Göttingen, Germany, 1997.

(43) Blessing, R. H. *Acta Crystallogr.* **1995**, *A51*, 33.

(44) Parkin, S.; Moezzi, B.; Hope, H. *J. Appl. Cryst.* **1995**, *28*, 53.

(45) Farrugia, L. J. *J. Appl. Cryst.* **1999**, *32*, 837.

(46) Speck, A. L. *Acta Crystallogr., Sect. A.* **1990**, *46, C.*

(47) Hirshfeld, F. L. *Acta Crystallogr., Sect. A.* **1976**, *32*, 239.

(48) Marques, L. L.; de Oliveira, G. M.; Lang, E. S. *Z. Anorg. Allg. Chem.* **2006**, *632*, 2310. - Reddy, H. K.; Cheng-Zhang; Shlemper, E. O.; Schrauzer, G. N. *Inorg. Chem.* **1992**, *31*, 1673. - Halasz, I.; Horvat, M.; Biljan, T.; Mestrovic, E. *J. Chem. Cryst.* **2008**, *38*, 793. - Defazio, S.; Cini, R. *Polyhedron* **2003**, *22*, 1355.

(49) Cordero, B.; Gómez, V.; Platero-Prats, A. E.; Revés, M.; Echeverria, J.; Cremades, E.; Barragán, F.; Alvarez, S. *Dalton Trans.* **2008**, 2832.

(50) Yamaguchi, T.; Yamazaki, F.; Ito, T. *J. Am. Chem. Soc.* **1999**, *121*, 7405.

(51) Szafert, S.; Gladysz, J. A. *Chem. Rev.* **2003**, *103*, 4175.

(52) Winter, M. *www.webelements.com: The Periodic Table on the W. W. W.*; The University of Shefield and Web Elements Ltd., U. K., 2008.

(53) Jeffrey, G. A. *An introduction to Hydrogen Bonding; Oxford University Press* **1997**.

(54) Lyssenko, K. A.; Antipin, M. Y. *Russ. Chem. Bull., Int. Ed.* **2006**, *55*, 1.

(55) Knope, K. E.; Cahill, C. L. *Inorg. Chem.* **2009**, *48*, 6845.

(56) Xie, J.; Abrahams, B. F.; Wedd, A. G. *Chem. Commun.* **2008**, 576.

(57) Reddy, L. S.; Chandrau, S. K.; George, S.; Babu, N. J.; Naugia, A. *Cryst. Growth Des.* **2007**, *7*, 2675.

(58) Chen, W.; Liu, F.; Nishioka, T.; Matsumoto, K. *Eur. J. Inorg. Chem.* **2003**, 4234.

(59) Femoni, C.; Kaswalder, F.; Iapalucci, M. C.; Longoni, G.; Zachini, S. *Chem. Commum.* **2006**, 2135.

(60) Umakoshi, K.; Saito, K.; Arikawa, Y.; Onishi, M.; Ishizaka, S.; Kitamura, N.; Nakao, Y.; Sakaki, S. *Chem. Eur. J* **2009**, *15*, 4238.

(61) Ford, P. C.; Cariati, E.; Bourassa, J. *Chem. Rev.* **1999**, *99*, 3625.

Table 1. Crystallographic Data for **1c(dmso)$_2$**·2CH_2Cl_2, **2a**·2CH_2Cl_2 and **2c**CH_2Cl_2.

	1c(dmso)$_2$·2CH_2Cl_2	**2a**·2CH_2Cl_2	**2c**·CH_2Cl_2
Empirical formula	C78 H72 Cd2 Cl4 O10 Pt2 S2	C42 H35 Cd Cl2 N Pt	C83 H68 Cd2 Cl2 N2 O8 Pt2
F_w	1990.26	932.10	1907.27
T (K)	173(1)	173(1)	173(1)
crystal system, space group	Monoclinic, P 2_1/n	Triclinic; P-1	Monoclinic, P 2_1/n
a(Å)	13.3388(4)	9.8650(2)	14.4841(4)
b(Å)	14.4103(8)	13.8180(3)	13.1672(4)
c(Å)	20.8566(12)	14.4500(3)	20.6477(3)
α(deg)	90	69.9970(10)	90
β(deg)	108.259(3)	81.6860(10)	91.4520(10)
γ(deg)	90	89.4250(10)	90
volume (A^3)	3807.1(3)	1829.82(7)	3936.56(17)
Z	2	2	2
D_{calcd} (Mg/m^3)	1.736	1.692	1.609
absorption coefficient (mm^{-1})	4.465	4.575	4.197
F(000)	1944	908	1860
θ range for data collection (deg)	3.25 to 25.68	2.09 to 27.89	3.38 to 25.68
no of data / restraints / params	7202 / 5 / 442	8671 / 0 / 437	7445 / 0 / 464
goodness-of-fit on $F^{2[a]}$	1.011	1.016	1.025
final R indexes $[I>2\sigma(I)]^{[a]}$	R1 = 0.0586, wR2 = 0.1232	R1 = 0.0347, wR2 = 0.0690	R1 = 0.0302, wR2 = 0.0776
R indexes (all data)$^{[a]}$	R1 = 0.1129, wR2 = 0.1442	R1 = 0.0491, wR2 = 0.0730	R1 = 0.0399, wR2 = 0.0827
largest diff peak and hole (e.$Å^{-3}$)	1.681 and -1.360	1.015 and -1.138	1.704 and -0.980

[a] $R1 = \Sigma(||F_o| - |F_c||)/\Sigma|F_o|$; $wR2 = [\Sigma w(F_o^2 - F_c^2)^2/\Sigma wF_o^2]^{1/2}$; goodness of fit = $\{\Sigma[w(F_o^2 - F_c^2)^2]/(N_{obs} - N_{param})\}^{1/2}$; $w = [\sigma^2(F_o) + (g_1P)^2 + g_2P]^{-1}$; $P = [\max(F_o^2;0 + 2F_c^2]/3$.

Table 1 Continued. Crystallographic Data for **4**·CH_2Cl_2 and **5**·2 acetone.

	4·CH_2Cl_2	**5**·2acetone
Empirical formula	C85 H66 Cd2 Cl2 F6 N2 Pt2	C42 H38 Cd N2 O Pt
F_w	1915.28	894.23
T (K)	173(1)	173(1)
crystal system, space group	Monoclinic, C 2/c	Triclinic; P-1
a(Å)	17.9732(5)	9.6288(4)
b(Å)	26.8534(8)	13.8741(5)
c(Å)	15.9466(4)	14.3504(6)
α(deg)	90	71.144(2)
β(deg)	102.5110(10)	80.783(2)
γ(deg)	90	87.744(2)
volume (A^3)	7513.7(4)	1790.62(12)
Z	4	2
D_{calcd} (Mg/m^3)	1.693	1.659
absorption coefficient (mm^{-1})	4.402	4.530
F(000)	3720	876
θ range for data collection (deg)	3.53 to 27.10	2.95 to 25.68
no of data / restraints / params	8276 / 6 / 454	6666 / 0 / 431
goodness-of-fit on $F^{2[a]}$	1.039	1.025
final R indexes $[I>2\sigma(I)]^{[a]}$	R1 = 0.0285, wR2 = 0.0654	R1 = 0.0455, wR2 = 0.1195
R indexes (all data)[a]	R1 = 0.0378, wR2 = 0.0698	R1 = 0.0483, wR2 = 0.1225
largest diff peak and hole ($e.Å^{-3}$)	1.109 and -1.360	2.623 and -2.553

[a] $R1 = \Sigma(||F_o| - |F_c||)/\Sigma|F_o|$; $wR2 = [\Sigma w(F_o^2 - F_c^2)^2/\Sigma wF_o^2]^{1/2}$; goodness of fit = $\{\Sigma[w(F_o^2 - F_c^2)^2]/(N_{obs} - N_{param})\}^{1/2}$; $w = [\sigma^2(F_o) + (g_1P)^2 + g_2P]^{-1}$; $P = [\max(F_o^2;0 + 2F_c^2]/3$.

Table 2: Selected Bond Lengths [Å] and Angles [deg] for **2a**·$2CH_2Cl_2$, **4**·CH_2Cl_2, **5**·2acetone, **2c**·CH_2Cl_2 and **1c(dmso)$_2$**·$2CH_2Cl_2$:

	2a·$2CH_2Cl_2$	**4**·CH_2Cl_2	**5**·2acetone	**1c(dmso)$_2$**·$2CH_2Cl_2$	**2c**·CH_2Cl_2
Pt(1)-Cd(1)	3.1186(3)	3.0872(3)	3.1289(5)	2.9053(8)	2.8001(4)
Pt(1´)-Cd(1)	2.6999(3)	2.7460(3)	2.6953(4)	2.9114(8)	2.8505(4)
Pt-C^{α}	2.005(3)-2.028(5)	2.001(3)-2.028(4)	1.992(6)-2.026(6)	2.007(10)-2.027(11)	2.010(4)-2.018(5)
Cd-C^{α}	2.436(5), 2.451(4)	2.409(4), 2.418(4)	2.423(7), 2.429(5)	2.470(10)-2.508(10)	2.471(5)-2.551(5)
Cd-C^{β}	2.669(5), 2.717(4)	2.645(4), 2.736(4)	2.643(6), 2.701(6)		
Cd-$C^{\alpha'}$	2.491(4)	2.475(5)	2.495(5)		
C^{α}-C^{β}	1.195(7)-1.227(5)	1.199(5)-1.209(5)	1.204(8)-1.215(8)	1.187(13)-1.207(13)	1.202(6)-1.213(6)
Cd(1)-N(1)	2.239(3)	2.277(3)	2.221(4)		2.245(4)
Cd(1)-O(5)				2.225(6)	
Cd(1)-Pt(1)-Cd(1´)	86.362(8)	91.772(9)	85.068(11)	102.27(2)	97.261(10)
Pt(1)-Cd(1)-Pt(1´)	93.638(8)	87.356(8)	94.933(11)	77.73(2)	82.740(10)
Pt-C^{α}-C^{β}	173.7(3)-177.1(4)	172.0(3)-175.2(3)	174.8(5)-178.2(5)	173.6(9)-175.4(9)	172.5(5)-178.8(4)
C^{α}-C^{β}-C^{γ}	172.7(4)-178.0(4)	171.2(4)-177.5(5)	172.3(6)-177.9(6)	173.4(12)-175.6(11)	171.0(5)-176.7(5)

Table 3: Emission data for complexes **1-5**.			
complex	Solid state λ^{em}_{max} /nm [τ/μs] {ϕ/%} 298 K	77 K	CH_2Cl_2 5×10^{-5} M (298 K) λ^{em}_{max} /nm [τ/μs]
1'a	[a]	514 [8.8]	[b]
1'b	[a]	525 [7.8]	[b]
1'c	[a]	468_{max}, 507*sh*	[b]
1a(acetone)$_2$	488 [13.5]	484, 512*sh* [14.3]	
1a	510 [12.7]	501 [13.0]	
1b(acetone)$_2$	515	489, 509*sh*	
1b	560 [10.7]	540 [11.4]	
1c(dmso)$_2$	500	492_{max}, 532*sh*	
2a	490 [8.0] {4.5}	479 [9.3]	533
2b	520 [7.2] {15.2}	500 [9.2]	[b]
2c	492 [14.5] {6.9}	469, 512*sh* [9.6]	528 [11.0]
3	488 [11.7] {10.5}	477, 512*sh* [17.6]	532
4	505 [14.1] {13.3}	506 [15.1]	546[c]
5	545 [10.2] {36.3}[d]	530 [8.7])[d]	567 [9.1]

[a] No emissive at 298 K. [b] No soluble. [c] Measured with excess of $NC_5H_4CF_3$-4 (1:10). [d] Measured over crystals containing acetone molecules (**5**·2acetone).

Table 4: Molecular Orbital Composition in terms of ligands and metals for complexes **1c(dmso)$_2$**, **2a**, **2c**, **4** and **5.**

	1c(dmso)$_2$				**2a**				**2c**				**4**				**5**			
MO	Pt	Cd	C≡CR	dmso	Pt	Cd	C≡CR	py	Pt	Cd	C≡CR	py	Pt	Cd	C≡CR	py	Pt	Cd	C≡CR	pzH
L+3	3	2	94	1	0	1	4	96	0	0	16	84	0	0	4	95	3	3	25	69
L+2	5	11	82	3	29	13	54	3	25	10	60	5	27	13	58	2	0	1	9	90
L+1	4	10	85	1	0	1	2	97	0	1	9	91	0	1	2	98	18	11	53	17
LUMO	22	11	67	0	0	1	2	97	0	1	9	91	0	1	2	98	29	13	58	1
HOMO	20	1	79	0	14	0	86	0	15	1	84	0	15	1	84	0	15	2	83	0
H-1	21	1	78	0	15	2	83	0	10	2	88	0	14	1	85	0	13	0	86	0
H-2	16	2	81	1	14	1	85	0	16	1	83	0	12	2	76	0	17	1	82	0
H-3	18	2	80	1	14	2	83	0	14	2	84	0	19	2	78	1	18	3	79	0

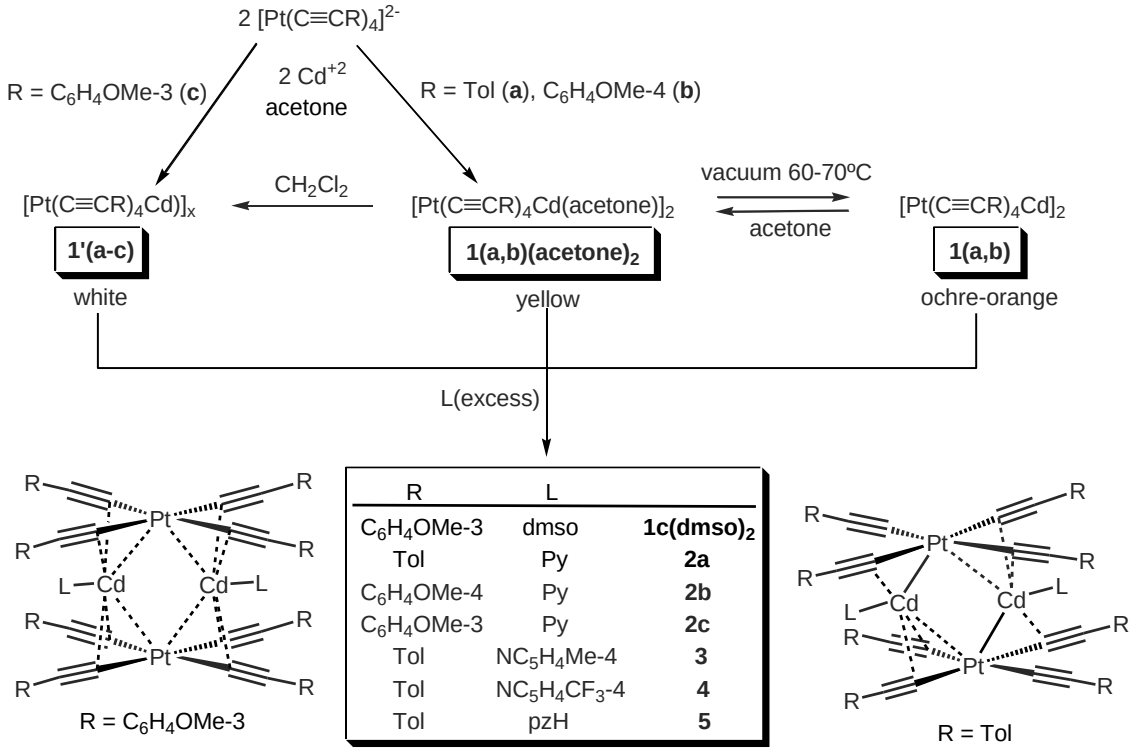

R	L	
C_6H_4OMe-3	dmso	**1c(dmso)$_2$**
Tol	Py	**2a**
C_6H_4OMe-4	Py	**2b**
C_6H_4OMe-3	Py	**2c**
Tol	NC_5H_4Me-4	**3**
Tol	$NC_5H_4CF_3$-4	**4**
Tol	pzH	**5**

Scheme 1

Figure Captions:

Figure 1: Molecular structure of $[Pt(C{\equiv}CTol)_4Cd(py)]_2$ **2a**. Only atoms of the central core ($Pt_2Cd_2(C{\equiv}C)_8$) are drawn as ellipsoids at 50 % probability level and hydrogen atoms omitted for clarity.

Figure 2: Molecular structure of $[Pt(C{\equiv}CTol)_4Cd(pzH)]_2{\cdot}2$acetone **5·**2acetone. Only atoms of the central core ($Pt_2Cd_2(C{\equiv}C)_8$) and nitrogens of the pyrazol ligand are drawn as ellipsoids at 50 % probability level, while hydrogen except H2, which is involved in H···O(acetone) contacts, are omitted.

Figure 3: Zenith view of the molecular structure of $[Pt(C{\equiv}CC_6H_4OMe\text{-}3)_4Cd(py)]_2$ **2c** (50 % probability ellipsoids). Aryl and pyridil atoms are simplified and hydrogen atoms are omitted for clarity.

Figure 4: Molecular structure of $[Pt(C{\equiv}CC_6H_4OMe\text{-}3)_4Cd(dmso)]_2$ **1c(dmso)$_2$**. Only atoms of the central core ($Pt_2Cd_2(C{\equiv}C)_8$) and dmso are drawn as ellipsoids at 50 % probability level and hydrogen atoms are omitted for clarity.

Figure 5: $^{195}Pt\{^1H\}$NMR spectra of **4** + $NC_5H_4CF_3$-4 (6 eq.) in CD_2Cl_2 at 298 K.

Figure 6: Absorption spectra of **1c(dmso)$_2$** in a mixture CH_2Cl_2:dmso (9:1) (pink) and **2a** (red), **2c** (black), **3** (blue) and **5** (orange) in CH2Cl2 (5×10^{-5} M).

Figure 7: Absorption spectra of freshly prepared solution of **1a(acetone)$_2$** (black) and **4** (dashed) in CH_2Cl_2 (5×10^{-5} M). In light grey, successive additions of 2, 6, 8, 18 and 38 equivalents of $NC_5H_4CF_3$-4 to the solution of **4**, showing the grew of the band at 376 nm and the appearance of a shoulder at 348 nm, together with the decrease of the band at 316 nm upon the addition of ligand.

Figure 8: Normalized emission spectra for solid samples of **1a(acetone)$_2$** (black), **1b(acetone)$_2$** (red) and **1c(dmso)$_2$** (blue) at 298 (solid line) and 77 K (dashed).

Figure 9: Emission spectra at room temperature of complexes **2a** (red), **2b** (light blue), **2c** (white), **3** (blue), **4** (green) and **5** (yellow) in the solid state (solid lines) and CH_2Cl_2 solution (dotted lines).

Figure 10: Frontier orbital plots for **2a** and **1c(dmso)$_2$** obtained by TD-DFT.

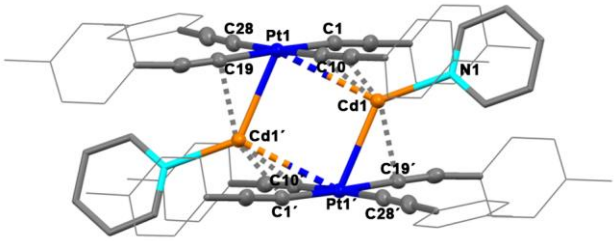

Figure 1

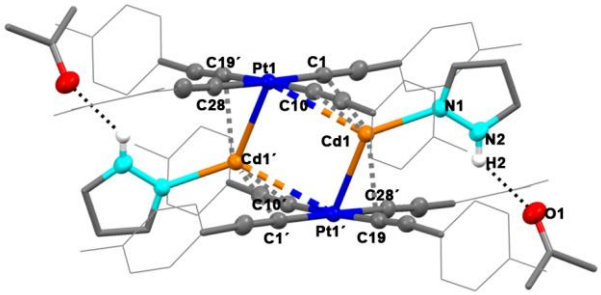

Figure 2

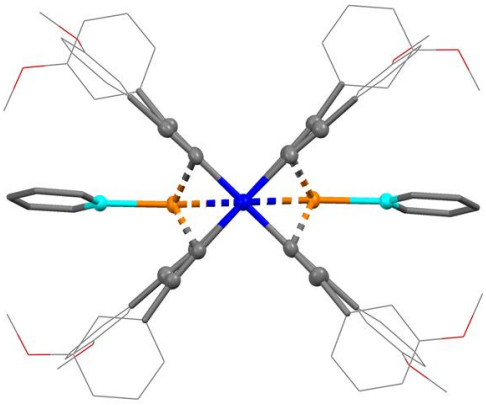

Figure 3

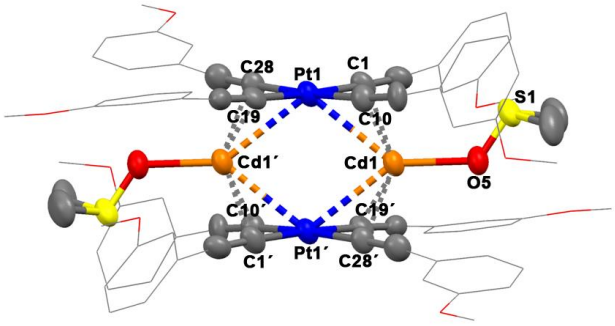

Figure 4

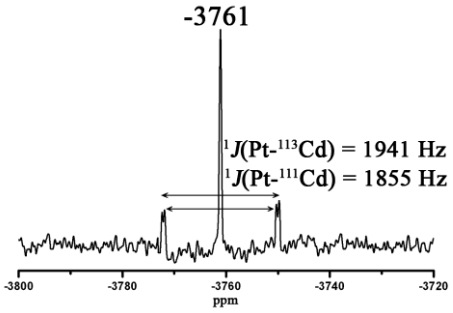

Figure 5

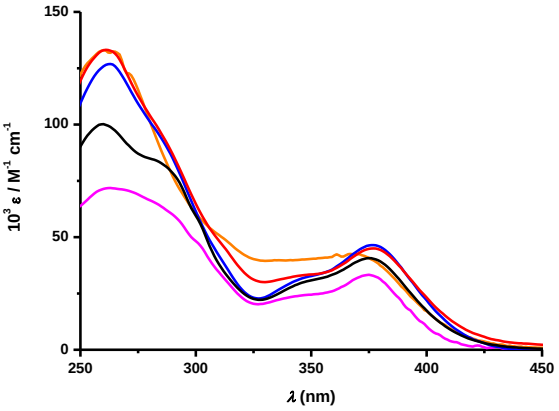

Figure 6

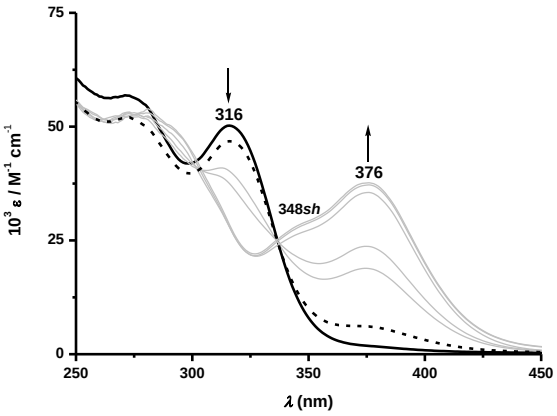

Figure 7

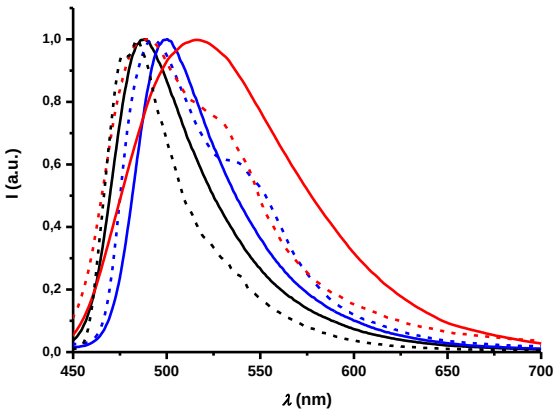

Figure 8

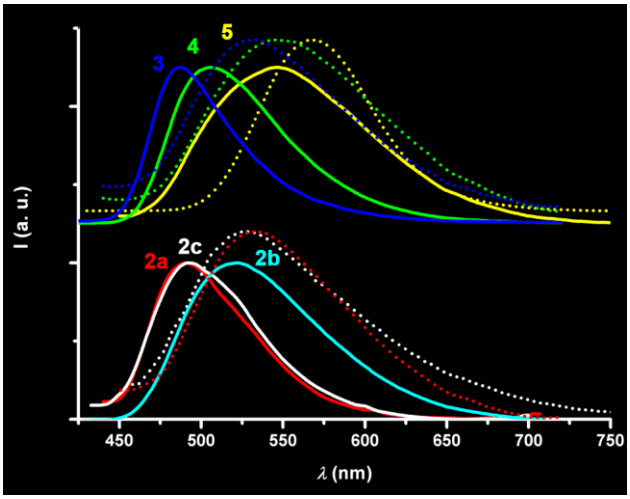

Figure 9

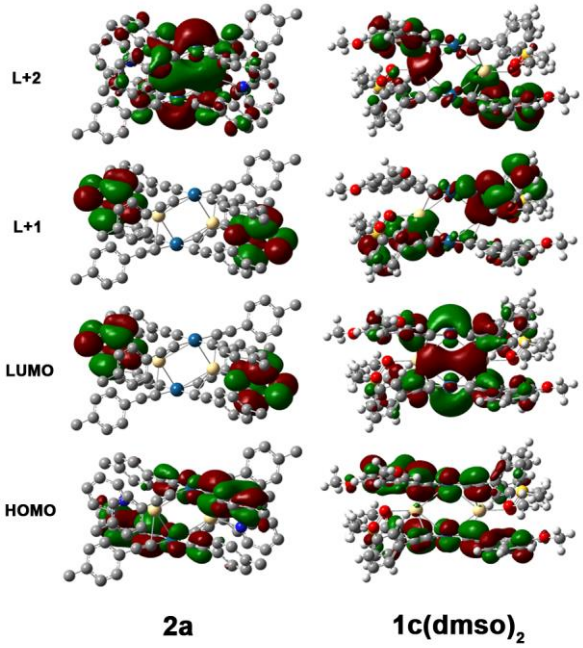

Figure 10

“for Table of Contents use only”

“Rombohedral heterometallic alkynyl based Pt_2Cd_2 clusters: Structural, photophysical and theoretical studies.”

Jesús R. Berenguer, Julio Fernández, Belén Gil, Elena Lalinde* and Sergio Sánchez.

Brightly luminescent rombohedral heterometallic $[Pt(C{\equiv}CR)_4CdL]_2$ (L = acetone, dmso, py, $NC_5H_4CH_3$-4, $NC_5H_4CF_3$-4, pzH) clusters, stabilized by a synergistic combination of Pt···Cd and Cd···alkynyl bonding interactions, have been prepared from $[Pt(C{\equiv}CR)_4]^{2-}$ and Cd^{2+}. Their photophysical properties have been examined and supported by DFT calculations.